J Mater Sci (2011) 46:4276–4283
DOI 10.1007/s10853-011-5303-4

IIB 2010

Nanostructurization assisted by twinning during equal channel angular pressing of metastable 316L stainless steel

H. Ueno · K. Kakihata · Y. Kaneko · S. Hashimoto · A. Vinogradov

Received: 25 August 2010 / Accepted: 18 January 2011 / Published online: 1 February 2011

Abstract A conventional SUS 316L low carbon stainless steel has been processed by Equal channel angular pressing (ECAP) to the equivalent shear strain equal to 2, 4, 6 or 8 at different temperatures ranging from 250 °C to room temperature. The aim of this study is to gain extra control over the "strength-ductility" combination via nanostructure formation, involving twinning and/or strain-induced phase transformation. The resultant microstructure is examined by transmission electron microscopy, X-ray diffraction and electron back scattered diffraction (EBSD) techniques. Substantial structure refinement down to nanoscale is observed in parallel with significant enhancement of tensile yield and ultimate tensile stress, both exceeding 1GPa. A considerable resistance to fracture during localized plastic flow and a fairly good elongation to fracture in tension is reported.

Introduction

The significance of grain boundaries and interfaces for materials properties cannot be overvalued. The amount of grain boundaries is governed by the grain size which therefore can be regarded as a key structural factor affecting nearly all aspects of the physical, chemical, and mechanical behavior of metals. Hence, control over the grain size has long been recognised as an avenue for designing materials with desired properties. Among the procedures devised for grain refinement, severe plastic deformation (SPD) techniques [1] have been proven capable of producing ultrafine grained (UFG) materials with sub-micron grain size range in bulk-scale work pieces after high imposed strains amounting up to 24 or so, thus increasing substantially the volume fraction of interfaces up to several or even ten percent and giving promise for structural applications.

The SUS 316L stainless steel is a material of particular interest because of its wide range of applications in the industry. Qu et al. [2] successfully obtained bulk nanocrystalline grain structures in low carbon stainless steel by means of ECAP at room temperature. TEM investigations showed that two types of nanostructures were formed: nanocrystalline strain-induced martensite with a mean grain size of 74 nm and nanocrystalline austenite with a size of 31 nm characterized by high density of deformation twins. This result suggests nanostructurization by ECAP benefits significantly from low stacking fault energy (SFE). Focusing on microstructure formation Belyakov et al. [3, 4] have deformed the 304 steel in uniaxial compression at elevated temperature. Dobatkin et al. [5, 6] have demonstrated the possibility of martensitic transformation during high pressure torsion of austenitic stainless steels. Yapici et al. [7] have deformed the 316L steel by ECAP at various temperatures ranging from 450 to 800 °C. They observed the increased tensile and compressive strength in parallel with SPD-induced miscrostructure refinement and deformation twinning.

One of major problems associated with UFG structures produced by SPD is their inherent thermal and mechanical instability caused by an excess amount of dislocations, local internal stresses and limited hardenability [8]. A variety of

H. Ueno
JTEKT Corporation, Osaka 582-8588, Japan

H. Ueno · K. Kakihata · Y. Kaneko · S. Hashimoto · A. Vinogradov (✉)
Department of Intelligent Materials Engineering, Osaka City University, Osaka 558-8585, Japan
e-mail: alexei@imat.eng.osaka-cu.ac.jp

ways have been proposed to stabilize deformed structures. These include alloying and enhancing the planarity of slip [9], forming a bimodal structure [10], intensifying twinning [11] and activating phase transformations either in a form of precipitations [12] or deformation-induced martensite [13]. Aid of twining and/or phase transformation is of particular interest for this study since both give rise to increasing strain hardening, preventing necking and thus maintaining a very high strain capacity. Potentially the use of the TWIP (Twining-induced plasticity) or TRIP (Transformation-induced plasticity) effect can give a clue for enhancement of ductility in UFG structures and provide an appealing way of tailoring UFG microstructures with different phase fractions and novel functional properties. Thus, another motivation of this study is to clarify whether the TWIP/TRIP effect is significant or not during ECAPing of the SUS 316L stainless steel.

Despite a large amount of papers generated during the past two decades in the field of SPD and a large number of materials processed, very few reports are available about mechanical properties linked to microstructure formation in a stainless steel. Greger et al. [14] have produced the UFG SUS 316L steel with twin layers in the microstrcuture by ECAP in the 105° die at temperatures up to 280 °C. After four pressings they have reached the σ_{02} and σ_{UTS} values exceeding 1 GPa, namely 1.063 and 1.099 GPa, respectively, and elongation to failure of 15%. The 316L stainless steel contains metastable austenite, which can be transformed to martensite during deformation (strain-induced martensite) below the M_d temperature. The volume fraction of deformation-induced martensite increases with increasing strain leading to substantial strengthening. Ucok et al. [15] produced the ultrafine-grained 316L stainless steel with the yield strength as high as 1280 MPa by heavy cold working at 77 K followed by annealing at 973 K. Pakiela et al. [16] prepared a nanostructured 316L with a grain size of 65 nm using high pressure torsion. This steel had a tensile strength of about 1340 MPa. A higher strength (up to 1920 MPa) can be obtained by deformation at cryogenic temperatures to achieve a 100% martensitic structure, however, the ductility will be completely sacrificed (less than 3% elongation to failure).

In this study the authors will show that a combination of high strength (up to 1600 ± 30 MPa) with good ductility (17% elongation at break and 36% cross-section area reduction) is possible by tailoring a microstructure by means of ECAP at modest temperature.

Experimental procedure

The nominal composition of the SUS 316L steel used in this study is shown in Table 1. The material was austenitized at 1080 °C for 5 min and water quenched. ECAP has been performed using a die with 4×4 mm^2 channels intersecting at 90° with sharp corner. The ECAP has been performed up to four passes via route Bc whereby the billet was rotated by 90° between subsequent passes. The pressing velocity was 0.1 mm/s and temperatures ranged from 250 °C to room temperature (250, 150, 80, 50, and 20 °C). The equivalent plastic strain imposed onto a working billet per pass for a given die geometry equals 1.15 (shear strain $\Gamma = 2$) [1].

The microstructure after ECAP was observed by a scanning electron microscope JEOL 6500-FEM equipped with the EDAX-TSL EBSD detector and by JEOL JEM 2100 transmission electron microscope operated at 200 kV. Several thin foils were obtained from the plane normal to the extrusion direction of the specimens and then examined in TEM to make sure that the observed microstructures are representative. The Rigaku Rint-2000 X-ray diffractometer was used with the filtered Co–K_α irradiation to study the phase composition and the lattice strain in the samples before and after ECAP.

Tensile tests were carried out on a screw-driven testing machine at a nominal strain rate 1×10^{-3} s^{-1}. After tensile failure, the dimensions of the final cross-section area were measured using microscopic images of the fracture surface. True fracture strain ε_b^T and true fracture stress σ_b^T were estimated from the fracture load and initial and final cross-sectional areas.

Results

Microstructure

The average grain size in the as received state was about 10 μm. The EBSD observations reveal a typical coarse grain austenitic structure with the presence of annealing twin boundaries and a small amount of bcc phase located primarily at the grain boundaries, Fig. 1a (shown in green; the EBSD phase map is shown in Fig. 1b where the fcc lattice is marked in red and the bcc lattice is marked in green). This bcc phase is commonly identified as retaining δ-ferrite, resulting in slight ferromagnetic properties.

Table 1 Chemical composition of the SUS 316L stainless steel

Element	C	Si	Mn	P	S	Ni	Cr	Mo	Fe
Amount (wt%)	0.008	0.62	1.19	0.033	0.002	12.09	17.33	2.04	Balance

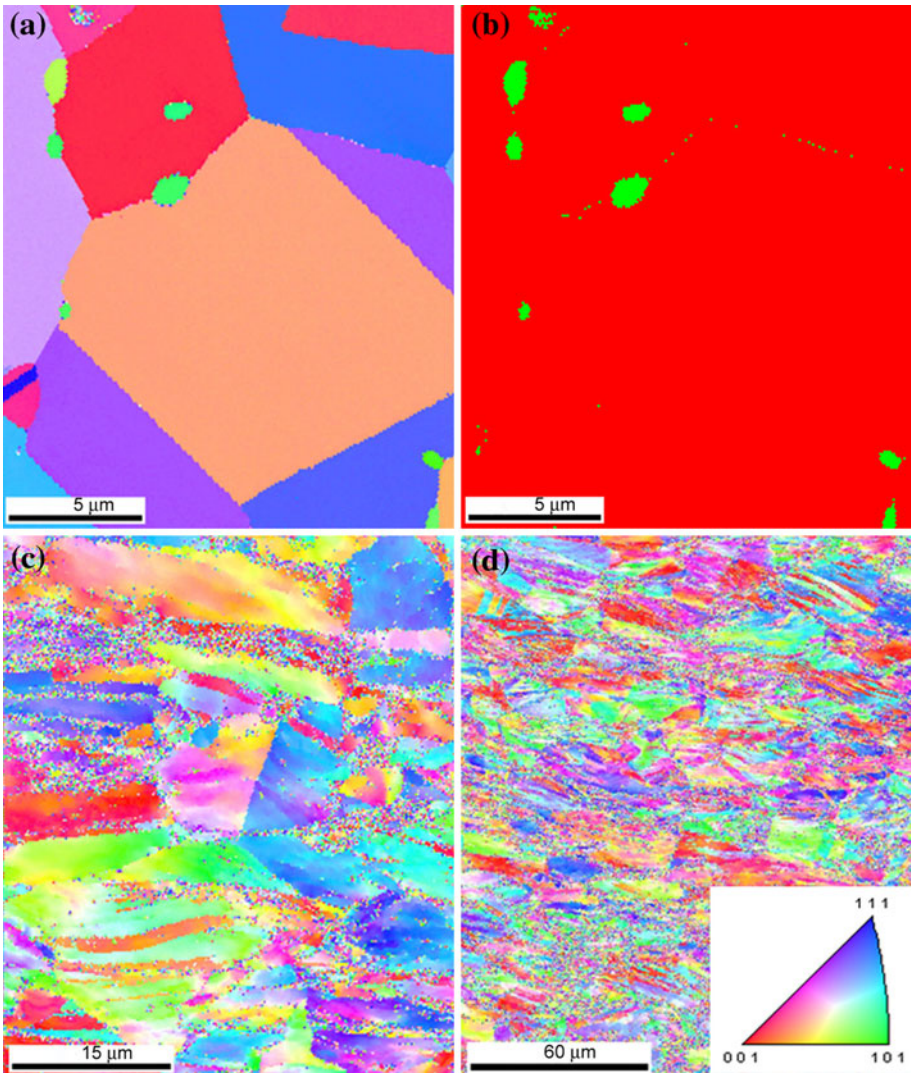

Fig. 1 Orientation maps of SUS 316L steel in the as-received state (**a**) and after 1 ECA-pass at 250 °C (**c**), and 150 °C (**d**); (**b**) the phase map corresponding image (**a**) the fcc lattice is marked in red and the bcc lattice in *green*

The traces of the δ-ferrite phase can be also found in the X-ray patterns, Fig. 2. The structure becomes considerably finer after the first ECA-pass and then refines further with the number of pressings. The structure after ECAP is characterized by large number of deformation bands with low and high angles of misorientation between adjacent domains, Fig. 1c and d. These bands divide the initial grains into fragments as is frequently observed during deformation of materials with relatively low SFE promoting planarity of slip. The lower processing temperature results in a finer structure and higher lattice strain, c. f. Fig. 1c and d. The latter manifests itself in blurred Kikuchi patterns which appeared unclear in local points, generating a high color noise on orientation image maps (OIM) and making the phase analysis by EBSD unclear.

Increasing lattice strain is also confirmed by the XRD analysis. After ECAP the X-ray peaks shift slightly to higher angles, Fig. 2a and broaden significantly, Fig. 2b. The ECAP induced broadening of the austenite peaks increases as working temperature reduces, which is characteristic of increasing lattice strain during SPD. Besides, the intensity of the austenitic peaks, e.g., (111), decreases after ECAP. This can be an indication of the phase transformation (partial transformation of γ phase into α' martensite) which might occur during ECAP. After ECAP at room temperature, a very weak X-ray maximum can be seen in the insert to Fig. 2a around $2\theta = 51.50^{o}$ where the bcc α' martensite (110) peak is expected. Nonetheless, the separation between γ and α' peaks is not clear enough to conclude firmly about the presence of martensite in the deformed structure.

The shift of the XDR peaks to higher angles indicates that the lattice parameter, a, of the austenite phase after ECAP reduces and the relative change $\Delta a/a_0$ related to the "unstrained" lattice constant, a_0, of as-received sample amounts to 0.5% after ECA-pressing at room temperature, giving rise to considerable residual stresses in the austenitic phase. As a general trend, the X-ray peak broadening in

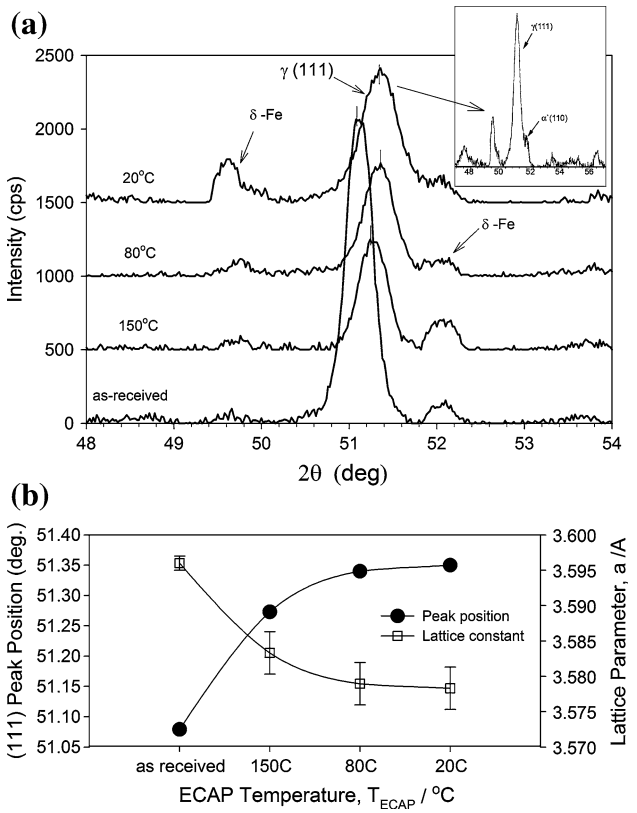

Fig. 2 XRD profiles, depending on the processing temperature (**a**). The shift of the γ-austenite (111) peak to higher angle and corresponding change of the lattice parameter (**b**)

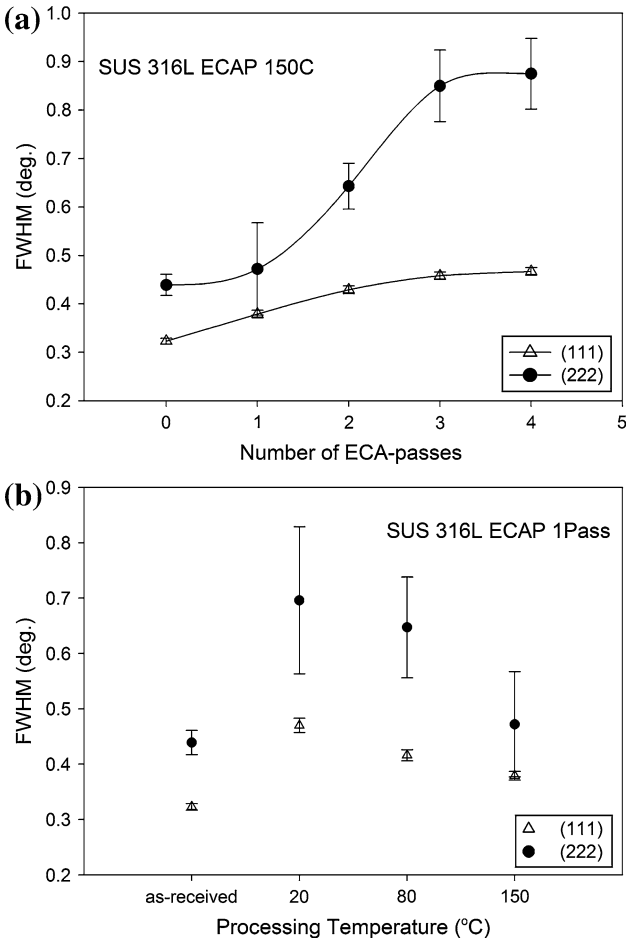

Fig. 3 X-ray austenite peak broadening depending on the number of ECA-passes at 150 °C (**a**) and processing temperature (**b**)

terms of the full width half maximum (FWHM) increases with the number of pressings, Fig. 3a and/or with the reduced processing temperature, Fig. 3b, which is associated with increasing working load and accumulating lattice strain during processing.

Figure 4 shows the bright filed TEM images and respective selected area electron diffraction patterns (SAEDP) of the 316L stainless steel ECAPed at 150 °C to 1 and 3 passes. The banded structure consisting of multiple mechanical twin layers having nanoscopic width is clearly evident after 1 ECA-pass. With further pressing to 3 passes via the "orthogonal" route Bc the intersection of the twinning systems is inevitable and elongated twin layers are divided into fragments having nanometer dimensions not only in width but also in length. Although the elongated grain structure with the aspect ratio of 2.5–3 is still visible in the deformed sample after 3 passes, Fig. 4c, a rather equiaxed structure with grains of 10–40 nm size is readily observed in large areas here and there in different sections across the sample, Fig. 4d (notice that Fig. 4d was obtained from the foil sectioned from the plane nrmal to the extrusion direction). It is possible to conclude that while the ultrafine grain structure with grain sizes of 200–500 nm forms in many materials during SPD, the nanostructure is common in the SPD-manufactured 316L austenitic stainless steel. The authors suppose that nanostructurization in this material is strongly assisted by twinning and possibly by formation of the martensitic phase at the intersection of the deformation bands.

Mechanical properties

Reduction of the processing temperature gives rise commonly to higher processing load and higher yield stress after ECAP. The tensile stress–strain curves are shown in Fig. 5 for the samples manufactures comfortably at 150 °C. Austenitic steels of 300 series are well known for their excellent ductility and relatively small necking elongations. Significant hardening after ECAP is paired by significant loss in ductility as is commonly observed in severely plastically deformed metals [17]. The elongation to failure reduces from 90% in the as received state to 30% after the first pass and then to 17% after four subsequent passes. The uniform elongation stage is short amounting to about 5% in all ECAPed samples, which is expected

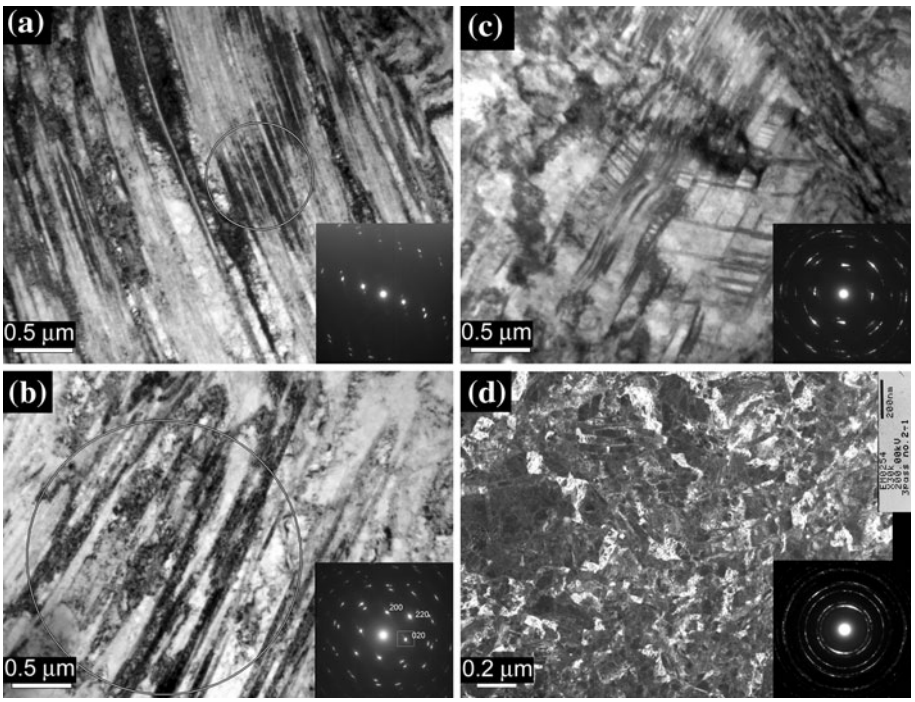

Fig. 4 Bright field TEM images of the microstructure in SUS 316L stainless steel ECAPed at 150 °C to 1 (**a**, **b**) and 3 (**c**, **d**) passes and corresponding SAEDP. The circles in (**a**) and (**b**) correspond to areas from which the SAEDP was obtained. Micrographs **a–c** were taken from the flow plane and **d** from the plane perpendicular to the extrusion direction

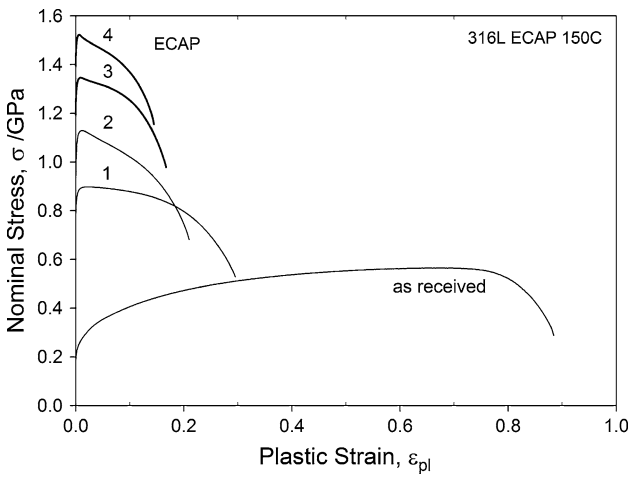

Fig. 5 Tensile stress strain curves of the SUS 316L stainless steel after ECAP at 150 °C

reasonably from limited hardenability after SPD in line with the Considère's criterion for the loss of the macroscopic stability and the onset of necking.

The prompt necking at yield resulting in low uniform elongation is a common feature of many SPD materials. However, localized deformation within the neck can be very prominent [18]. SEM observations of the fracture surface of the steel studied reveal ductile dimple-like fracture relief and the sample view after fracture is shown in Fig. 6 showing that the present ECAPed steel is featured by a fairly large area reduction at break (c.f. Table 2), indicating fairly high local ductility and crack nucleation resistance in the neck.

It is well known, that the mechanical properties, strength and uniform elongation, can be improved considerably in the post-SPD thermo-mechanical treatment involving either deformation or hear treatment or a combination of both (e.g., [19]). The positive effect of annealing is associated with relaxation of internal stresses, optimization of grain boundary structure and partial recovery of dislocations introduced during SPD. In this study the authors did not explore the full capacity of post-ECAP treatment aiming at structure optimization and enhancement of properties and this will be done in future studies.

Discussion

Austenitic steels of 300 series exhibit a great variety of deformation mechanisms: besides the dislocation glide, the TWIP and TRIP effects are common phenomena for these steels depending on their chemical composition. As has been mentioned above, the occurring deformation mechanisms are closely related to SFE of the austenitic phase. In general, the tendency toward martensite formation increases with amount of chromium, strain, deformation speed, and decreases with nickel equivalent, SFE and deformation temperature. The SFE in austenitic stainless steels of 300 series varies broadly from low to high values: 9.2–80.7 mJ/m^2 [20]. Frommeyer et al. [21] concluded that at the SFE lower than 16 mJ/m^2 the $\gamma \rightarrow \alpha'$-transformation is the favored mechanism, whereas the SFE above 25 mJ/m^2 supports twinning and above 60 mJ/m^2 plastic deformation

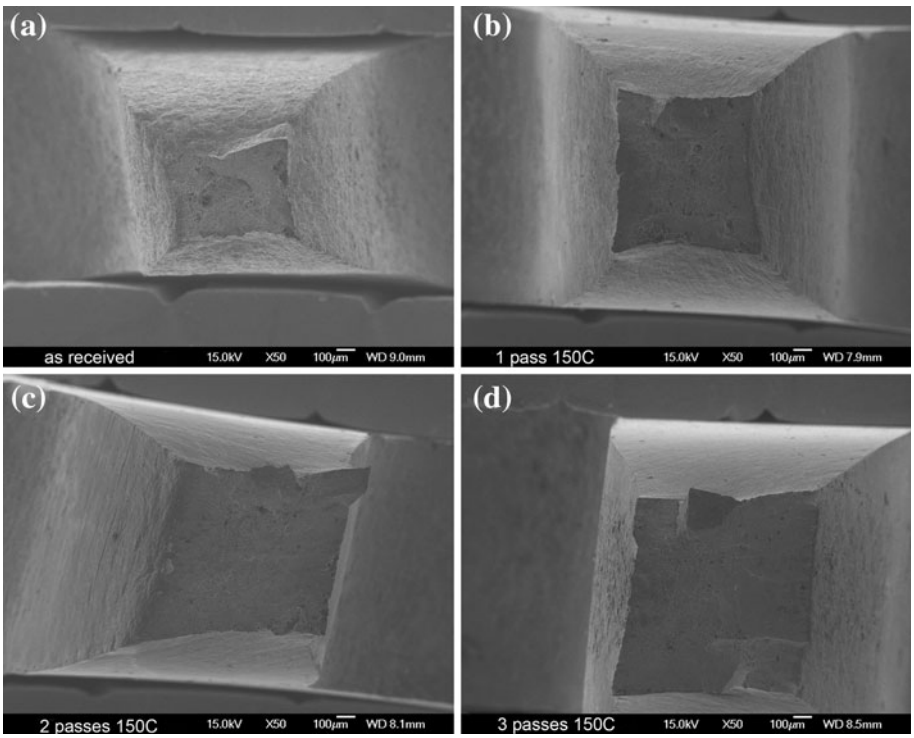

Fig. 6 Fracture surface (tensile) of 316L stainless steel ECAPed at 150 °C after tensile test: **a** as received, **b** 1 ECA-pass, **c** 2 passes **d** 3 passes

Table 2 Mechanical properties of SUS316L stainless steel ECAPed at 150 °C

Sample	σ_{02}, MPa	σ_{UTS}, MPa	ε_U	ε_b	AR (%)	σ_b^T, MPa
0 passes (as-received)	220	560	0.75	0.88	80 ± 5	1460 ± 20
1 pass 150 °C ECAP	850	900	0.05	0.30	73 ± 4	1530 ± 50
2 passes ECAP	1040	1120	0.05	0.20	60 ± 5	1700 ± 80
3 passes ECAP	1300	1440	0.05	0.18	52 ± 3	1770 ± 50
4 passes ECAP	1480	1560	0.05	0.17	44 ± 2	2050 ± 30

σ_{02} conventional nominal yield stress, σ_{UTS} ultimate nominal tensile strength, ε_U uniform elongation, ε_b- elongation at break, σ_b^T true stress at break

is mediated by dislocation slip. Depending on the chemical composition the SFE can be estimated by the following empirical relation [22]:

$$\begin{aligned}\mathrm{SFE}\left[{}^{\mathrm{mJ}}/_{\mathrm{m}^2}\right] &= 25.7 + 2\cdot \mathrm{Ni} + 410\cdot C - 0.9\cdot \mathrm{Cr} \\ &\quad - 77\cdot \mathrm{N} - 13\cdot \mathrm{Si} - 1.2\cdot \mathrm{Mn} \end{aligned} \quad (1)$$

The chemical composition also determines the austenite phase stability. The parameters commonly used to express the austenite stability are the martensite start temperature, M_s and the M_{d30} -temperature, which represents the lowest temperature where 50% of deformation-induced α'-martensite is formed with a true strain of 30%. The lower parameters indicate the higher respective austenite stability, and vice versa: the greater the M_{d30}, the more unstable the austenite should be. The empiric relationships for estimating the values of M_s and M_{d30} are given by Eichelmann and Hull [23] and Angel [24], respectively, as:

$$\begin{aligned} M_s[^\circ\mathrm{C}] &= 1350 - 1665\cdot(\mathrm{C}+\mathrm{N}) \\ &\quad - 28\cdot\mathrm{Si} - 33\cdot\mathrm{Mn} - 42\cdot\mathrm{Cr} - 61\cdot\mathrm{Ni} \\ M_{d30}[^\circ\mathrm{C}] &= 413 - 462\cdot(\mathrm{C}+\mathrm{N}) - 9.2\cdot\mathrm{Si} - 8.1\cdot\mathrm{Mn} \\ &\quad - 13.7\cdot\mathrm{Cr} - 9.5\cdot\mathrm{Ni} - 18.5\cdot\mathrm{Mo} \end{aligned} \quad (2)$$

From the alloy chemistry (Table 1), Eqs. 2 and 3 yield a medium SFE of 28 mJ/m^2 for the steel under investigation and M_s and M_{d30} temperatures of −185 and 119 °C, respectively. The M_s temperature is quite low and therefore martensite formation is not expected during initial cooling from 1080 °C. However, the M_{d30} temperature is high enough to expect some martensitic transformation at room temperature or possibly a small amount of martensite can

be produced after intensive multi-pass ECA-straining even at 150 °C processing temperature.

Mechanical twinning occurs usually at high strains and low temperatures. However, the propensity of twining is promoted by solutes raising the shear stress in the slip plane, reducing SFE and increasing the planarity of slip. Similarly, martenistic transformation $\gamma \rightarrow \alpha'$ or $\gamma \rightarrow \varepsilon \rightarrow \alpha'$ tends to occur at lower temperatures, and it is also promoted by lower SFE. Using TEM of the deformed 316LN steel Byun et al. [25] have shown that twins, stacking faults, and/or martensite laths, along with dislocations, are formed at subzero temperatures and dislocation-dominant microstructures at elevated temperatures.

Byun [26] reported that during deformation of 316 stainless steels a variety of deformation structures is produced depending on the reached stress level: (1) dislocation tangles were dominant at low equivalent stresses of 400 MPa; (2) isolated stacking faults smaller than about 1 μm were formed in the stress range from about 400–600 MPa; (3) twin bands became dominant at stresses exceeding 600 MPa at room temperature. It was argued that the critical twinning stress is proportional to the stacking fault energy, which is a positive function of temperature. Hence, the temperature dependence of the SFE determines the temperature dependence of critical twinning stress σ_T [27]. During the first ECA-pressing through the die at 150 °C, the steady extrusion occurred in these experiments at maximum normal stress of 900–1000 MPa that exceeds the critical twinning stress of 750 MPa expected at this temperature [27]. During the third pass, the normal stress reaches 2.3–2.5 GPa which is by far higher than σ_T.

Mechanical twining depends on grain size, easier twinning being expected at larger grain sizes [28], i.e., deformation twins can be most efficient at first pressings through the die. It is timely to notice that formation of a distinctive banded twin structure, Fig. 4a and b, with characteristic orientation splitting seen on the SAEDP correlates with particularly high ductility in the neck and high strength at fracture after first and second path. Dislocation glide and twinning are competitive mechanisms of plastic deformation: the second comes into play when the first exhausts and cease to accommodate the imposed strains. The dislocation multiplication in very fine grains can be impeded so that twinning can be a major mechanism of plastic flow [29]. Alternatively, martensitic transformation may also occur during deformation in parallel with twinning as was observed by Mishra et al. [30].

An interesting finding of this study is related to the ability of the ECAPed 316L steel to deform significantly during necking. Table 2 and Fig. 6 shows that although the cross-section area reduction decreases with the number of ECA-passes from about 80% in the as received state to 44% after 4 passes, the local ductility in the neck still remains high. Accordingly, the true stress at break increases from about 1460 to 2050 MPa indicating thereby that the local strain hardening capacity remains high too. The detailed mechanism of this hardening has yet to be understood. Bearing in mind a potential application of this material for nuclear engineering, Wu et al. [27] have discussed that certain irradiation conditions lead to the development of a damaged microstructure where plastic flow is confined to very small volumes of material, as opposed to the smooth plastic flow observed in unirradiated materials. In other words, the observed high resistance of the ECAPed SUS 316L stainless steel to the localized plastic flow even at high stresses can be of interest for prospective applications.

Summary and conclusions

(i). Austenitic stainless steel SUS 316L has been subjected to severe plastic deformation by ECAP at different temperatures aiming at forming ultra-fine grained structures. Deformation bands consisting of multiple twin layers with nanoscopic width and length limited by a grain dimensions have been commonly observed after the first pass through the die at elevated temperature (150 °C). The twining activated during the first ECA-passes is supposed to play a key role in nanostructurization during further ECAP processing.

(ii). A uniform nanostructure has been proven to form after the third ECA-pass (route Bc) at 150 °C.

(iii). Following a general trend, the yield strength increased significantly after the first ECA-pressing and then kept increasing steadily with increasing accumulated strain during further pressing. An appealing combination of the strength and ductility has been demonstrated though a short uniform deformation stage (5% plastic strain) is still below expectations.

A challenging goal to make use of the TRIP and/or TWIP effect to delay necking and extend the uniform ductility has yet to be achieved and this will be the scope of the future research.

Acknowledgements This study was financially supported by the Grant-in-Aid for Scientific Research on Innovative Area, "Bulk Nanostructured Metals", through MEXT, Japan (contract no. 22102006), and this support is gratefully appreciated.

References

1. Azushima A, Kopp R, Korhonen A, Yang DY, Micari F, Lahoti GD, Groche P, Yanagimoto J, Tsuji N, Rosochowski A, Yanagida A (2008) CIRP Annal Manufact Technol 57(2):716

2. Qu S, Huang CX, Gao YL, Yang G, Wu SD, Zang QS, Zhang ZF (2008) Mater Sci Eng A 475(1–2):207
3. Belyakov A, Sakai T, Miura H (2001) Mater Sci Eng A 319:867
4. Belyakov A, Sakai T, Miura H (2000) Mater Trans Jim 41(4):476
5. Dobatkin SV, Zrník J, Mamuzić I (2006) Metalurgija 45(4):313
6. Dobatkin SV, Rybal'chenko OV, Raab GI (2006) Russ Metal 2006(1):42
7. Yapici GG, Karaman I, Luo ZP, Maier HJ, Chumlyakov YI (2004) J Mater Res 19(8):2268
8. Miyamoto H, Mimaki T, Vinogradov A, Hashimoto S (2002) Annales de Chimie—Science des Matériaux 27:S197
9. Zhao YH, Zhu YT, Liao XZ, Horita Z, Langdon TG (2006) Appl Phys Lett 89 (12) p 121906
10. Wang Y, Chen M, Zhou F, Ma E (2002) Nature 419(6910):912
11. Zhu YT, Liao XZ, Wu XL (2008) Jom 60(9):60
12. Vinogradov A, Patlan V, Suzuki Y, Kitagawa K, Kopylov VI (2002) Acta Mater 50(7):1639
13. Dobatkin SV (2003) In: On the increase of thermal stability of ultrafine grained materials obtained by severe plastic deformation. Thermec'2003, Pts 1–5 426–4:2699
14. Greger A, Kander L, Kocich R (2008) Arch Mater Sci Eng 31(1):41
15. Üçok I, Ando T, Grant NJ (1991) Mat Sci Eng A 133:284
16. Pakiela Z, Garbacz H, Lewandowska M, Druzycka-Wiencek A, Sus-Ryszkowska M, Zielinski W, Kurzydlowski KJ (2006) Nukleonika 51:S19
17. Zhu YT, Liao X (2004) Nat Mater 3(6):351
18. Vinogradov AY, Stolyarov VV, Hashimoto S, Valiev RZ (2001) Mater Sci Eng A 318:163
19. Huang X, Kamikawa N, Hansen N (2010) J Mat Sci 45:4761. doi:10.1007/s10853-010-4521-5
20. Padilha AF, Plaut RL, Rios PR (2003) ISIJ International 43(2):135. doi:10.2355/isijinternational.43.135
21. Frommeyer G, Brüx U, Neumann P (2003) ISIJ International 43(3):438. doi:10.2355/isijinternational.43.438
22. Pickering F (1985) In: Conference of stainless steels, Goteborg. The institute of metals, London p 2
23. Eichelmann GH, Hull FC (1953) Trans Am Soc Met 45:77
24. Angel T (1954) J Iron Steel Inst 177:2
25. Byun TS, Hashimoto N, Farrell K (2004) Acta Mater 52(13):3889
26. Byun TS (2003) Acta Mater 51(11):3063
27. Wu X, Pan X, Mabon JC, Li M, Stubbins JF (2006) J Nucl Mater 356(1–3):70
28. Meyers MA, Murr LE (1978) Acta Metal 26(6):951
29. Liao XZ, Zhao YH, Srinivasan SG, Zhu YT, Valiev RZ, Gunderov DV (2004) Appl Phys Lett 84(4):592
30. Mishra S, Narasimhan K, Samajdari I (2007) Mater Sci Technol 23(9):1118